


# Reproducibility of Native T<sub>1</sub> Mapping for Renal Tissue Characterization at 3T

Ilona A. Dekkers, MD, MSc <sup>1\*</sup>, Elisabeth H.M. Paiman, MD,<sup>1</sup>  
Aiko P.J. de Vries, MD, PhD,<sup>2</sup> and Hildo J. Lamb, MD, PhD<sup>1</sup>

**Background:** Advanced renal disease is characterized by adverse changes in renal structure; however, noninvasive techniques to diagnose and monitor these changes are currently lacking.

**Purpose:** To evaluate the reproducibility of native T<sub>1</sub> mapping for renal tissue characterization.

**Study Type:** Reproducibility study.

**Population:** Fifteen healthy volunteers (mean age 31 years, range 19–63 years), and 11 patients with diabetic nephropathy (mean age 57 years, range 51–69 years).

**Field Strength/Sequence:** 3T, modified Look–Locker imaging (MOLLI) 5(3)3.

**Assessment:** Intra- and interexamination reproducibility of voxel-based T<sub>1</sub> relaxation times of renal cortex and medulla was assessed in healthy human volunteers and diabetic nephropathy patients.

**Statistical Tests:** Reproducibility was evaluated using Bland–Altman and intraclass correlation coefficients (ICCs).

**Results:** Intra- and interexamination reproducibility of renal native T<sub>1</sub> mapping showed good–strong ICCs (0.83–0.89) for renal cortex and medulla, and moderate–good ICCs (0.62–0.81) for cortex–medulla ratio in both healthy volunteers and diabetic nephropathy patients. Intra- and interexamination limits of agreement were respectively (–124 msec, + 82 msec) and (–134 msec, + 98 msec) for renal cortex and (–138 msec, + 107 msec) and (–118 msec, + 151 msec) for medulla. Overall T<sub>1</sub> values for renal cortex ( $P = 0.277$ ) and medulla ( $P = 0.973$ ) were not significantly different between healthy volunteers and diabetic nephropathy patients, in contrast to the cortex–medulla ratio ( $P = 0.003$ ).

**Data Conclusion:** Renal native T<sub>1</sub> mapping is a technique with good–strong intra- and examination reproducibility in both healthy volunteers and diabetic nephropathy patients.

**Level of Evidence:** 3

**Technical Efficacy:** Stage 1

J. MAGN. RESON. IMAGING 2019;49:588–596.

Renal disease often progresses unnoticed, as clinical biomarkers, such as glomerular filtration rate (GFR) and albuminuria, tend to deteriorate only late in the disease course.<sup>1</sup> There is an increasing need for the development of noninvasive imaging biomarkers that can help to predict clinical and functional outcomes in renal disease, and guide clinical decision-making.<sup>2</sup>

Renal disease is characterized by adverse changes in both renal macrostructure (renal volume and corticomedullary differentiation) and microstructure (renal inflammation, fibrosis, and lipid fat fraction).<sup>3</sup> These alterations in renal structure or renal tissue composition may be useful for differentiating specific renal disease states, and monitoring

disease activity over time. Magnetic resonance imaging (MRI) has the ability to discriminate tissue composition using T<sub>1</sub> (spin-lattice) relaxation properties. Recent technical advances have enabled noninvasive tissue characterization via pixelwise mapping of true T<sub>1</sub> values of the target organ of interest, without the use of contrast agents. This so-called native T<sub>1</sub> mapping, in which color-coded pixel values represent the corresponding T<sub>1</sub> relaxation times per voxel, has been used in cardiac MRI to visualize myocardial fibrosis, steatosis, edema, and hemosiderosis.<sup>4</sup>

Previous clinical studies have shown that native T<sub>1</sub> mapping could be helpful for identifying acute kidney injury and prediction of chronic kidney disease in mice.<sup>5–7</sup>

View this article online at [wileyonlinelibrary.com](http://wileyonlinelibrary.com). DOI: 10.1002/jmri.26207

Received Sep 1, 2017, Accepted for publication May 15, 2018.

\*Address reprint requests to: I.A.D., Albinusdreef 2, 2333 ZA Leiden, The Netherlands, C-02S. E-mail: [i.a.dekkers@lumc.nl](mailto:i.a.dekkers@lumc.nl)

From the <sup>1</sup>Department of Radiology, Leiden University Medical Center and Leiden University, Leiden, the Netherlands; and <sup>2</sup>Division of Nephrology, Department of Medicine, Leiden University Medical Center and Leiden University, Leiden, the Netherlands

This is an open access article under the terms of the Creative Commons Attribution-NonCommercial License, which permits use, distribution and reproduction in any medium, provided the original work is properly cited and is not used for commercial purposes.

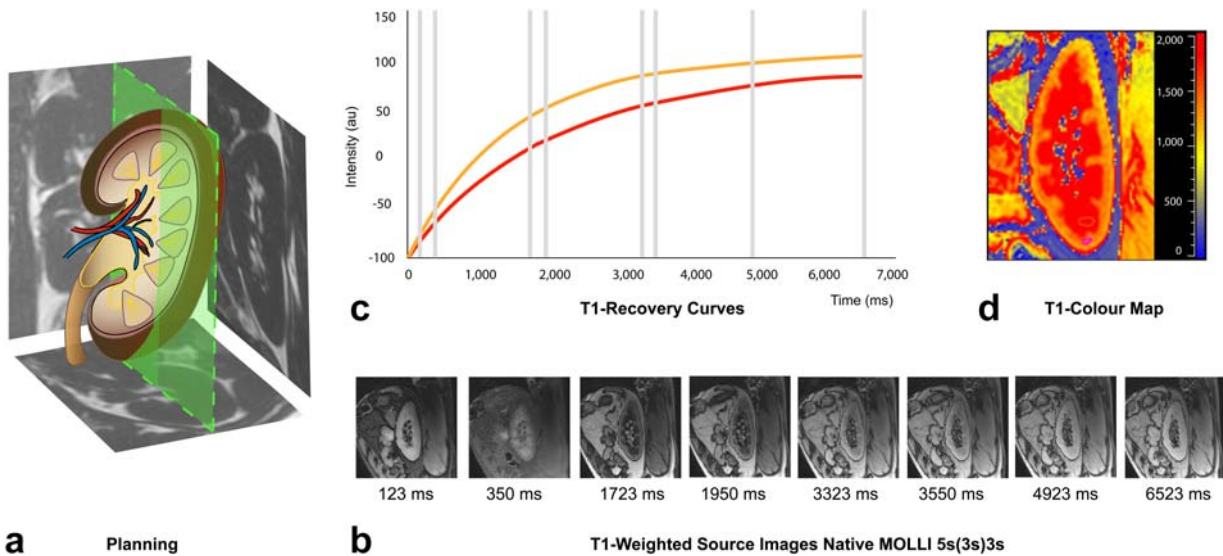


**FIGURE 1:** Planning and acquisition protocol of native MOLLI 5(3)3. **A:** Planning of T<sub>1</sub> mapping in the sagittal plane based on three orthogonal on mDixon images. **B:** T<sub>1</sub>-weighted source images in sagittal plane taken at different times (msec) after an inversion pulse at time  $t = 0$  for MOLLI 5(3)3, all acquired during a single breath-hold. **C:** Inversion recovery curves for renal cortex (orange) and medulla (red) generated from the source images. **D:** Generated color-encoded T<sub>1</sub> map in which pixel values represent corresponding T<sub>1</sub> relaxation times per voxel.

Additionally, recent human clinical studies have shown promising results of renal native T<sub>1</sub> mapping for the detection of fibrosis and prediction of graft functioning after kidney transplantation.<sup>8,9</sup> Given the considerable influence of the imaging protocol, scanner, and patient-related factors on measured T<sub>1</sub> values, evaluation of reproducibility and robustness is critical.<sup>10</sup> The purpose of the present study was to evaluate the reproducibility of native T<sub>1</sub> mapping for renal tissue characterization at 3T in healthy volunteers and diabetic nephropathy patients.

## Materials and Methods

### Participants

The Institutional Review Board of our institution approved the study protocol for MR technique development, and written informed consent was obtained from all participants. Fifteen healthy volunteers (mean age  $31 \pm 15$  years, range 19–63, 67% male) without known renal disease agreed to participate in the current study and were recruited from a database of healthy volunteers who regularly participate in technical MRI development studies. Eleven subjects with a known history of diabetic nephropathy (mean age  $57 \pm 8$  years, range 51–69, 80% male, urinary albumin excretion ratio  $>2.5$  mg/mmol for men or  $>3.5$  mg/mmol for women, and estimated GFR  $>60$  ml/min/1.73 m<sup>2</sup>) agreed to participate in the present study and were recruited from a database of past clinical trial participants.

### Data Acquisition

MR examinations were performed with a 3T clinical MRI scanner (Ingenia, Philips, Best, The Netherlands). The standard cardiac/body coil was used for transmission with two arrays (anterior and posterior with respectively 16 and 12 elements) for reception. After a breath-hold survey was obtained, three orthogonal modified

Dixon scans were acquired of the left kidney. T<sub>1</sub> mapping was performed using the modified Look–Locker inversion-recovery (MOLLI) sequence at the center of the kidney in sagittal orientation (Fig. 1A). The MOLLI sequence is a pulse scheme that allows for accurate in vivo T<sub>1</sub> measurements and pixelwise mapping of the T<sub>1</sub> values of the target organ of interest with high spatial resolution and within a single breath-hold.<sup>11</sup> This imaging scheme was used without the application of contrast media in the present study (referred to as native T<sub>1</sub> mapping). The sagittal orientation was chosen, as this orientation is less prone to through-plane volume effects compared to the coronal orientation while maintaining an overview of the upper and lower poles of the kidney, which is useful for evaluating the presence of local differences. Breath-holds were used for respiratory motion compensation. A turbo field echo (TFE) prepulse with an inversion delay of 350 msec was the longest (and last) inversion delay in the MOLLI scheme. Other inversion times in the MOLLI scheme were equidistantly distributed between shortest and longest value, according to the 5(3)3 cardiac MR protocol. Since the cardiac 5(3)3 protocol is normally electrocardiographically gated, we used the physiology simulator (Philips) to ensure scan triggering by simulating cardiac triggering in order to apply the protocol for renal imaging. The shortest inversion time was used for the first part of the MOLLI scheme and depended on the TFE shot duration, which is around 100 msec. Finally, eight images were acquired, and in-line motion correction and map generation were performed. Readout parameters were: slice thickness 8 mm; spacing between slices 8 mm; field of view  $300 \times 300$  mm; matrix  $256 \times 256 \times 1$  slice; pixel size  $1.17 \times 1.17$  mm. Intraexamination reproducibility measurements were obtained by repeating the scan without repositioning of the subject or changing the position of the surface coil or measurement volumes. Interexamination reproducibility was assessed on the same day after removal and repositioning of the subject in the magnet, and repositioning of the surface coil and measurements volumes.

Interexamination scans were added later in the scan protocol and were therefore not assessed in all healthy volunteers. Total acquisition time including positioning of the subject, scanning preparatory sequences, planning, and data acquisition was on average 4 minutes.

### **$T_1$ Mapping Quantification**

Eight  $T_1$ -weighted source images were taken at different times (msec) after an inversion pulse at time  $t = 0$  for MOLLI 5(3)3 during a single breath-hold (Fig. 1B). Postprocessing was done using QMap Research Edition (Medis, Leiden, the Netherlands) using received data in DICOM format. Inversion recovery curves were constructed for renal cortex (red) and medulla (orange) based on MOLLI images with varying effective inversion time (TI) with one series containing multiple images (Fig. 1C).

$T_1$  mapping was based on the three-parameter curve fitting of the data using the Levenberg–Marquardt algorithm, which is based on the equation  $A - B \cdot \exp(-x/T_1)$ , where A, B, and  $T_1$  are constants determined by curve-fitting the model to acquired phases. Offset, scaling, and  $T_1$  were calculated via fitting the algorithm at each pixel  $\{x,y\}$ , resulting in additional offset, scaling, and  $T_1$  maps. The color-encoded pixel-based  $T_1$  maps provide a quantitative visualization of the tissue  $T_1$  properties since the signal intensity of each pixel directly reflects the relaxation time calculated in milliseconds (Fig. 1D). The offset, scaling, and  $T_1$  maps were used to calculate additional R squared ( $R^2$ ) and residual maps for quality control, where good quality is reflected by  $R^2$  values and low residual values. The  $R^2$  map corresponds to the coefficients of determination, which lies between 0 and 1000, as the DICOM images store integer values only. The residual map was calculated based on the sum of squared differences between the fitted intensity value and the original image normalized for the number of image frames. The  $R^2$  and residual error map are sensitive to poor fitting due to motion-related artifacts, and spatial variation in off resonance due to  $B_0$ -field inhomogeneity. In case it was necessary, manual motion correction was performed.

Freehand region of interest (ROI)-based measurements were made for the mean  $T_1$  values by manually drawing small sample ROIs in the renal cortex and medulla of the lower pole of the left kidney (Fig. 2). Both renal cortex and medulla showed minimal regional differences and limited variance (SD) of the small sample ROI measurements. The outer borders of the kidney were not included in ROI measurements, since the outer border between renal parenchyma and perirenal fat or renal sinus fat are prone to gradual changes in  $T_1$  values due to partial volume averaging artifacts and possible residual registration error after motion correction. Banding artifacts in the kidney due to off-resonance were avoided by shifting these outside the kidney regions, since these artifacts can cause significant error at relatively small off-resonance frequencies.<sup>12</sup> The cortex–medulla ratio was determined by dividing the (ROI-based) native  $T_1$  value of renal cortex by the native  $T_1$  value of the medulla.

### **Statistical Analysis**

$T_1$  values and other descriptors are presented as mean (SD), range, and percentage. The Shapiro–Wilk test and assessment of histogram plots was applied to determine whether the data were

normally distributed and to select appropriate parametric tests. Pearson's correlation, and intraclass correlation coefficients (ICC) were calculated for intra- and interexamination measurements. The ICC can be interpreted as the ratio of the between-subject variance compared to the total variance (sum of the between-subject and within-subject variances) and was computed using a two-way mixed effects model.<sup>12</sup> Interobserver agreement was determined in a small subset of 14 subjects consisting of healthy volunteers as diabetic nephropathy patients by two blinded raters. Agreement was classified as follows: ICC >0.95; excellent, 0.95–0.85; strong, 0.85–0.70; good, 0.70–0.50; moderate, <0.5; poor. Bland–Altman plots were constructed for intra- and interexamination measurements and were visualized through a scatterplot of the differences, with reference lines at the mean difference, and mean difference  $\pm 2 \times$  standard deviation of the differences (limits of agreement).<sup>14</sup>

Two-tailed  $P < 0.05$  was considered to indicate a statistically significant difference. Statistical analyses were performed using STATA v. 12.0 (Statacorp, College Station, TX).

### **Results**

The overall results regarding the mean  $T_1$  values, Pearson correlation, and ICCs for first, intra-, and interexamination scans are presented in Table 1. Overall mean  $T_1$  values of healthy volunteers were  $1418 \pm 73$  msec (range 1270–1482 msec) for renal cortex and  $1886 \pm 86$  msec (range 1695–2006 msec) for medulla. One outlier was observed for the first  $T_1$  measurement in renal medulla (1600 msec) in the healthy volunteer group due to noncompliance regarding breath-hold instruction and remaining residual registration error after motion correction (Fig. 3). Overall mean  $T_1$  values of diabetic nephropathy patients were  $1445 \pm 81$  msec (range 1392–1545 msec) for renal cortex and  $1840 \pm 79$  msec (range 1751–2003 msec) for medulla. The overall mean cortex–medulla ratio was  $0.75 \pm 0.03$  (range 0.70–0.80) for healthy volunteers and  $0.79 \pm 0.03$  (range 0.74–0.82) for diabetic nephropathy patients. No significant differences were present when comparing  $T_1$  values for renal cortex ( $P = 0.277$ ) and medulla ( $P = 0.73$ ) of healthy volunteers with diabetic nephropathy patients. The cortex–medulla ratio was significantly different between healthy volunteers and diabetic nephropathy patients ( $P = 0.003$ ) (Fig. 3). Intra- and interexamination measurements were highly correlated with first  $T_1$  value measurements of renal cortex and medulla.

Intraexamination ICCs of renal cortex and medulla for both healthy volunteers and diabetic nephropathy patients combined were respectively 0.89 (95% confidence interval [CI] 0.75, 0.95) and 0.89 (95% CI 0.76, 0.95). Interexamination ICCs for renal cortex and medulla were 0.83 (95% CI 0.56, 0.93) and 0.83 (95% CI 0.57, 0.93). The cortex–medulla ratio had an intraexamination ICC of 0.62 (95% CI 0.16, 0.83) and 0.81 (95% CI 0.52, 0.93).

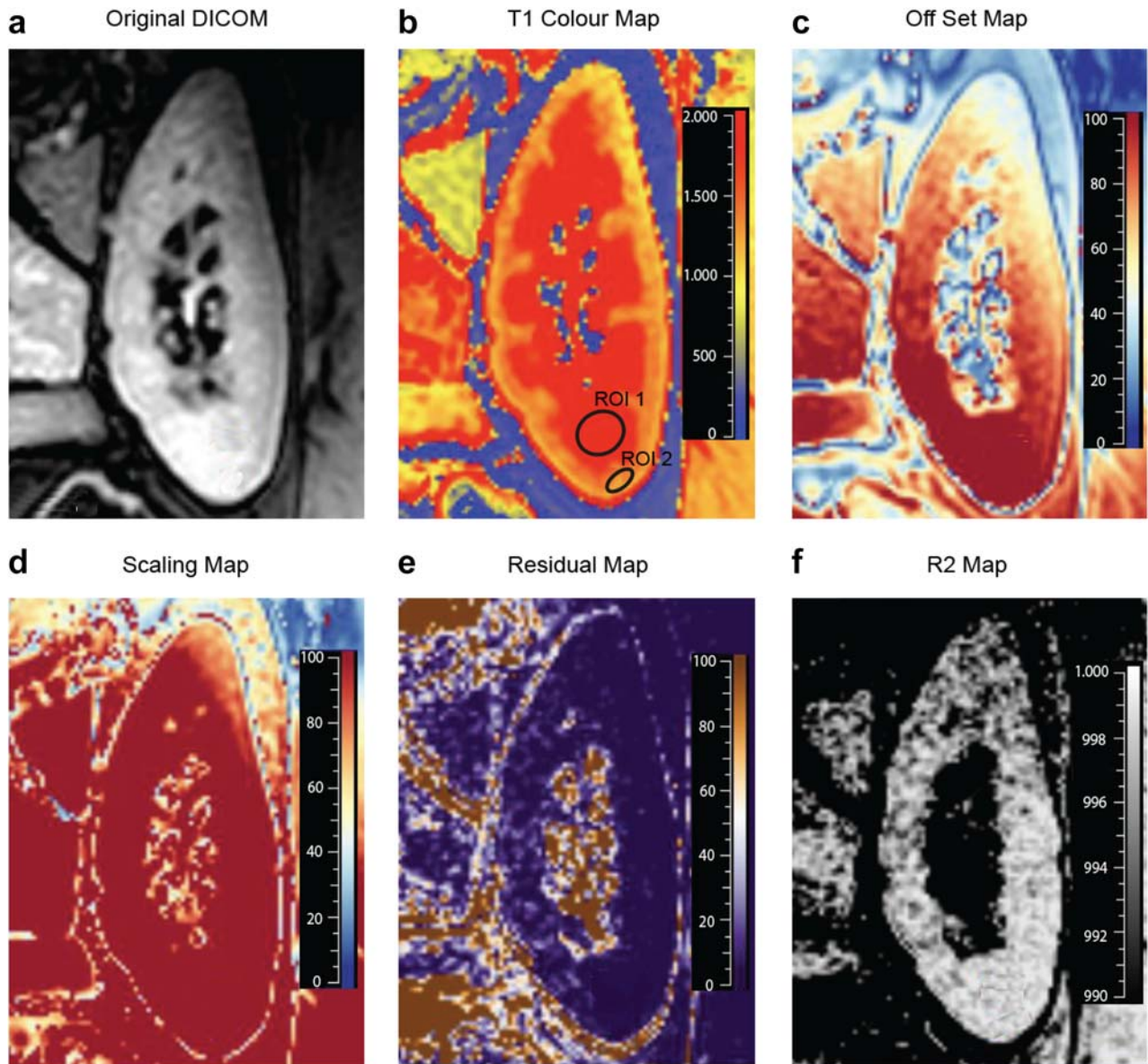


**FIGURE 2: ROI measurements for renal cortex and medulla on original DICOM, T<sub>1</sub> Color Map, Offset Map, Scaling Map, Residual Map, R<sup>2</sup> Map. A:** Original DICOM image of the MOLLI 5(3)3 sequence in sagittal plane of the left kidney. **B:** Color-encoded pixel based T<sub>1</sub> map with free-hand ROI measurements in renal cortex and medulla of the lower pole of the kidney. **C:** Offset map corresponds to the plateau value of the function, which should be equal to the last timepoint of the MOLLI 5(3)3 sequence. **D:** Scaling map, which ideally should be twice the value of the offset because then the T<sub>1</sub> is equal to the apparent recovery time T<sub>1</sub>\*. **E:** residual map reflects the sum of squared differences between the fitted intensity value and the original image normalized for the number of image frames. **F:** R<sup>2</sup> map corresponds to the coefficients of determination, which lies between 0 and 1000, because the DICOM images store only integer values.

The Bland–Altman lower and upper limits of agreement for intraexamination and interexamination T<sub>1</sub> measurements of renal cortex were respectively –124 msec (95% CI –159, –88) and 82 msec (95% CI 47, 118), and –134 msec (95% CI –181, –87) and 98 msec (95% CI –51, 145) (Fig. 4A,B). Intra- and interexamination Bland–Altman lower and upper limits of agreement for renal medulla were –138 msec (95% CI –180, –96), 107 msec (95% CI 65, 149) (Fig. 4C,D), and –118 msec (95% CI –172, –63), 151 msec (95% CI 96, 205). Cortex–medulla ratio measurements had lower and upper limits of agreement of –0.08

(95% CI –0.11, –0.06) and 0.07 (95% CI 0.05, 0.10) for intraexamination measurements, and –0.09 (95% CI –0.12, –0.06) and 0.06 (95% CI 0.03, 0.08) for interexamination measurements (Fig. 4E,F). Interobserver agreement analysis for 14 subjects and two blinded raters resulted in ICCs of 0.72 (95% CI 0.34, 0.90) for renal cortex and 0.42 (95% CI 0.15, 0.77) for medulla.

To illustrate the potential application of renal T<sub>1</sub> mapping, we have visualized coronal renal T<sub>1</sub> maps of a healthy volunteer (left), and renal transplant recipient (right) in Fig. 5. The renal T<sub>1</sub> map the healthy volunteer has T<sub>1</sub> values of

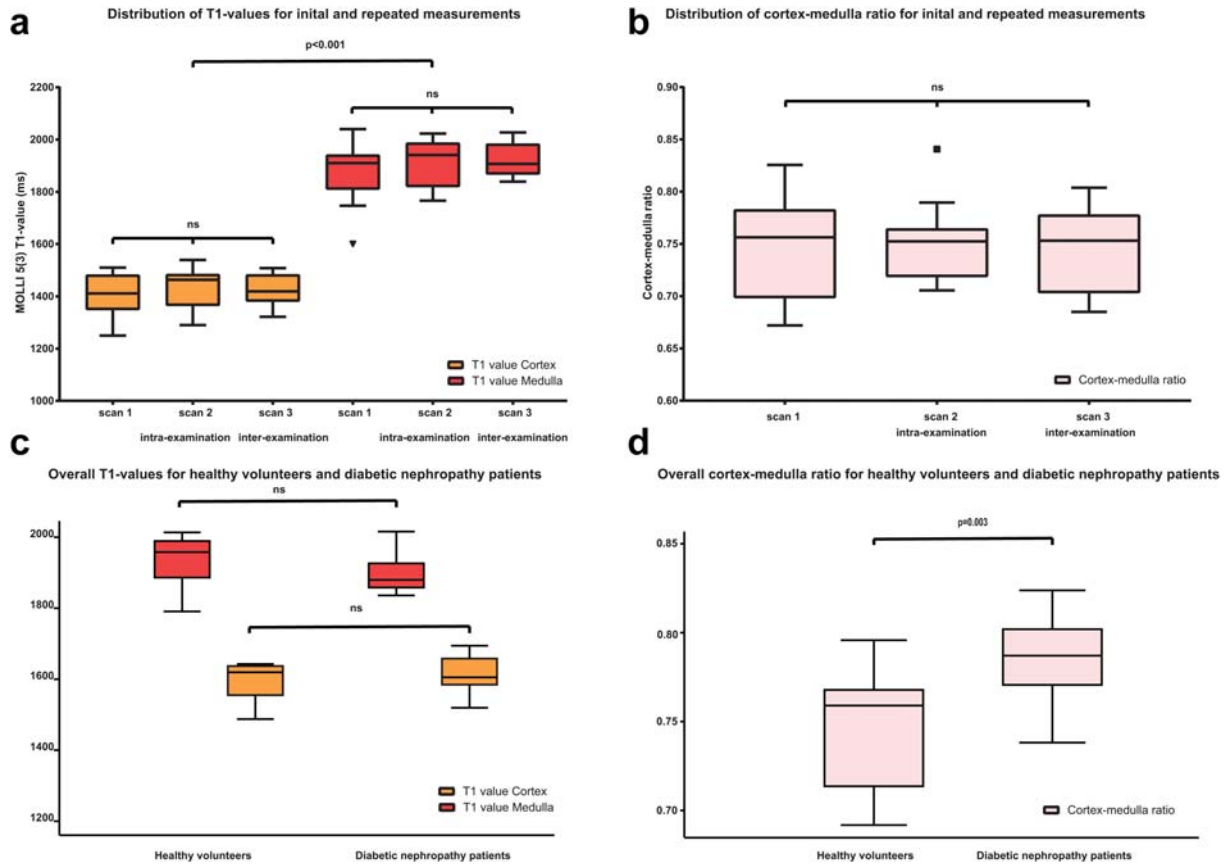


**FIGURE 3:** Distribution of MOLLI 5(3) ROI-based  $T_1$  values of renal cortex, medulla, and cortex–medulla ratio for first, intra-, and interexamination measurements. **A:** Distribution of  $T_1$  values of renal cortex (orange) and medulla (red) for first scan and repeated intra- and interexamination scans in healthy volunteers. **B:** Distribution of cortex–medulla ratio (pink) based on first scan and repeated intra- and interexamination scans in healthy volunteers. **C:** Overall  $T_1$  values for healthy volunteers (left) and diabetic nephropathy patients (right) for renal cortex (orange) and renal medulla (red). **D:** Overall cortex–medulla ratio (pink) for healthy volunteers (left) and diabetic nephropathy patients (right).

1468 msec in the renal cortex, and 1941 msec for medulla (cortex–medulla ratio of 0.76), compared to native  $T_1$  values of 1658 msec for renal cortex and 1951 msec for medulla (cortex–medulla ratio of 0.85) in the transplanted kidney.

### Discussion

We demonstrated that renal native  $T_1$  mapping using the MOLLI 5(3)3 sequence is a reproducible technique that could be used for renal tissue characterization.

The intra- and interexamination reproducibility of measured renal  $T_1$  values are an important determinant of the clinical utility of pixelwise  $T_1$  mapping for disease assessment. We evaluated the reproducibility of  $T_1$  measurements in renal cortex, renal medulla, and for the cortex–medulla ratio. Both intra- and interexamination ICCs ranged between moderate–strong in healthy volunteers and diabetic nephropathy patients separately. Intra- and interexamination ICCs for both groups combined were respectively 0.89 and 0.83 for both renal cortex and renal medulla, indicating strong intraexamination reproducibility. This is supported by the Bland–Altman plots showing good agreement.

One outlier was present in the intra- and interexamination Bland–Altman plots, which is likely the same healthy volunteer with residual motion artifacts due to noncompliance to breath-hold instructions during the data acquisition of scan 1. In general, ICC values were higher for renal medulla compared to cortex. The cortex is likely more sensitive for trough-plane partial volume effects than the medulla based on its anatomical borders and relatively limited thickness. This could potentially be improved via high-resolution 3D  $T_1$  mapping or via the use of postprocessing techniques such as automated motion correction of residual motion artifacts. The cortex–medulla ratio had ICCs ranging between moderate–good, indicating that this is a less reliable measure than  $T_1$  values directly measured in renal cortex and medulla.

Conventional MRI of the kidney clearly demonstrates anatomical differences between renal cortex and medulla due to the shorter  $T_1$  relaxation times of the cortex. Loss of this so-called corticomedullary differentiation occurs in several renal diseases and has been primarily attributed to altered  $T_1$  relaxation times in the renal cortex.<sup>15</sup> Determination the cortex–medulla ratio using true native  $T_1$  values of

**TABLE 1. Mean T<sub>1</sub> Values, Pearson Correlation, and ICCs for First, Intra-, and Interexamination Scans**

	Healthy volunteers			Diabetic nephropathy patients			Combined		
	Scan 1 N= 15	Intraexamination scan N= 9	Interexamination scan N= 11	Scan 1 N= 11	Intraexamination scan N= 11	Interexamination scan N= 11	Scan 1 N= 26	Intraexamination scan N= 26	Interexamination scan N= 20
T1 value (msec)									
Cortex	1408 ± 80	1437 ± 78	1427 ± 62	1433 ± 88	1445 ± 82	1449 ± 80	1419 ± 83	1440 ± 78	1861 ± 85
Medulla	1882 ± 108	1912 ± 83	1923 ± 63	1850 ± 89	1846 ± 100	1810 ± 65	1868 ± 100	1883 ± 95	1439 ± 72
CM ratio	0.75 ± 0.05	0.75 ± 0.03	0.74 ± 0.04	0.77 ± 0.03	0.78 ± 0.03	0.80 ± 0.04	0.76 ± 0.04	0.77 ± 0.03	0.77 ± 0.05
Pearson correlation (r)									
Cortex	0.65	0.49	0.49	0.96	0.96	0.79	0.80	0.80	0.71
Medulla	0.80	0.88	0.88	0.85	0.85	0.66	0.80	0.80	0.71
CM ratio	0.36	0.65	0.65	0.38	0.38	0.58	0.45	0.45	0.70
ICC (95% CI)									
Cortex	0.79 (0.37, 0.93)	0.66 (-0.51, 0.86)	0.66 (-0.51, 0.86)	0.98 (0.93, 0.99)	0.98 (0.93, 0.99)	0.88 (0.55, 0.97)	0.89 (0.75, 0.95)	0.89 (0.75, 0.95)	0.83 (0.56, 0.93)
Medulla	0.87 (0.62, 0.96)	0.91 (0.56, 0.98)	0.91 (0.56, 0.98)	0.91 (0.70, 0.98)	0.91 (0.70, 0.98)	0.77 (0.14, 0.94)	0.89 (0.76, 0.95)	0.89 (0.76, 0.95)	0.83 (0.57, 0.93)
CM ratio	0.52 (-0.44, 0.84)	0.79 (0.06, 0.95)	0.79 (0.06, 0.95)	0.55 (-0.57, 0.87)	0.55 (-0.57, 0.87)	0.70 (-0.14, 0.92)	0.62 (0.16, 0.83)	0.62 (0.16, 0.83)	0.81 (0.52, 0.93)

T<sub>1</sub> values are expressed as mean ± SD. CM ratio, cortex-medulla ratio; ICC, intraclass correlation coefficient.

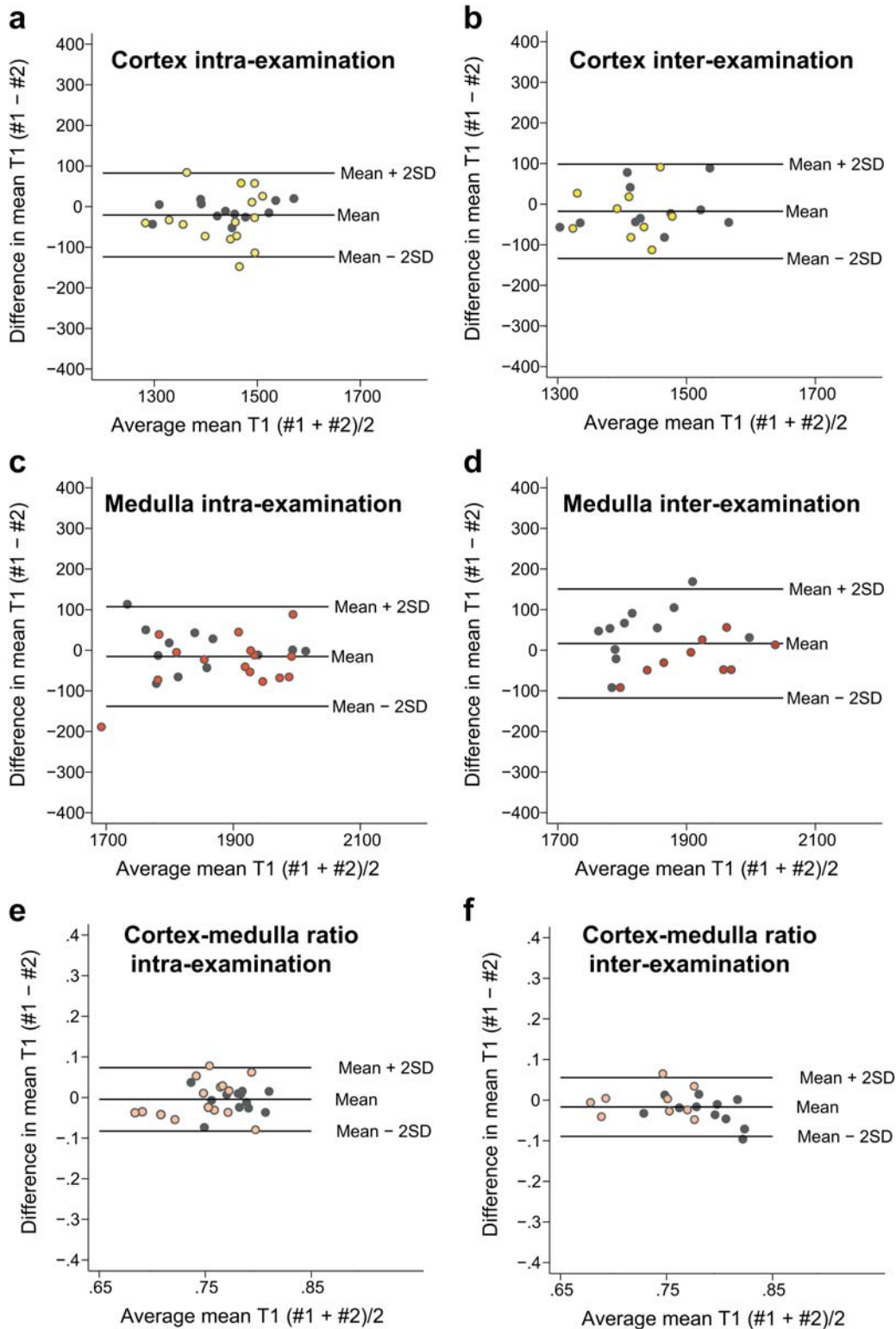


**FIGURE 4:** Bland–Altman plots of intraexamination and interexamination  $T_1$ -measurements of renal cortex (a, b) medulla (c, d) and cortex–medulla ratio (e, f) in healthy volunteers (in color) and diabetic nephropathy patients (in black).

renal cortex and medulla enables quantification of the corti-comedullary differentiation, which might be useful for differentiating specific renal disease states, such as renal fibrosis. In the present study,  $T_1$  values of renal cortex and medulla ranged respectively between 1270–1482 msec and 1695–2006 in healthy volunteers at 3T. Since native  $T_1$

values are considered to reflect both cellular components as interstitium, we postulate that the found differences between cortical and medullary  $T_1$  values convey anatomical differences in the renal (tubular)interstitium, which is defined as the extravascular, extraglomerular, and (inter)tubular space of the kidney.<sup>16</sup> Renal interstitial volume, in contrast to

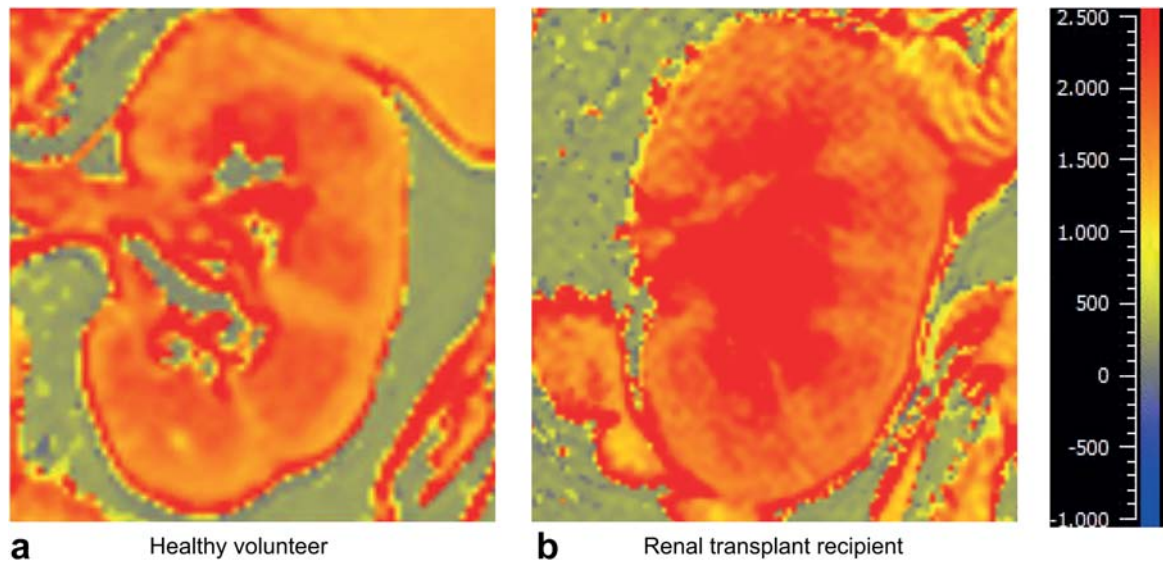


**FIGURE 5:** Coronal T<sub>1</sub> map of healthy volunteer (left), and T<sub>1</sub> map of renal transplant recipient (right). **A:** T<sub>1</sub> map of a kidney of a healthy volunteer in coronal view with values of 1468 msec for renal cortex, 1941 msec for medulla, and a cortex–medulla ratio of 0.76. **B:** Renal T<sub>1</sub> map of a renal transplant patient with an eGFR of 56 ml/min/1.73m<sup>2</sup> at time of scanning; native T<sub>1</sub> values were 1658 msec for renal cortex, 1951 msec for medulla, and a cortex–medulla ratio of 0.85.

severity of glomerular disease, is highly correlated with kidney function,<sup>17,18</sup> and can occupy over 60% of kidney tissue in severe renal disease.<sup>19,20</sup> Recently, it has been showed by Friedli et al that renal native T<sub>1</sub> values correlate well with renal fibrosis stage based on histology, suggesting that native renal T<sub>1</sub> might be a useful parameter to detect (subclinical) renal fibrosis.<sup>8</sup> Another very recent study in renal transplant recipients found prolonged T<sub>1</sub> values after transplantation and increased cortical T<sub>1</sub> values in higher stages of renal functional impairment,<sup>9</sup> indicating the potential use for prediction of graft survival/functioning. However, to what extent native T<sub>1</sub> mapping could be used as a safe noninvasive alternative for diagnosis and follow-up of renal disease remains to be further investigated.

Several limitations are present in this study that need to be considered. Since native T<sub>1</sub> mapping is at least partially modulated by perfusion (which is also a major determinant of GFR), T<sub>1</sub> relaxation times obtained in patients with impaired renal function could potentially be confounded by lower renal perfusion rather reflecting true fibrosis only. This could also have important implications when using other T<sub>1</sub>-mapping-based techniques such as arterial spin labeling, which could potentially limit the application of these techniques in the kidney. More research is needed to determine to what extent native renal T<sub>1</sub> values are affected by altered perfusion; however, we expect that current reproducibility measurements are minimally influenced by differences in renal perfusion since the study population consists of healthy volunteers and diabetic nephropathy patients with an eGFR >60 ml/min/1.73m<sup>2</sup>. Furthermore, in the present study we used manual placement of small-sized circular ROIs in order to obtain T<sub>1</sub>

values reflecting renal cortex and medulla separately, as these are clearly distinctive anatomical regions with important functional differences. A disadvantage of the present ROI analysis is potential user-dependency, as reflected in the interobserver agreement analysis, which resulted in ICCs of 0.72 for renal cortex T<sub>1</sub> values and 0.42 for renal medulla. In the present study the aim was to evaluate the reproducibility of renal T<sub>1</sub> mapping rather than assessing differences between healthy volunteers and renal disease patients. T<sub>1</sub> values of renal cortex and medulla were not significantly different between healthy volunteers and renal disease patients, in contrast to the cortex–medulla ratio. These findings should be interpreted with caution, as the assessment of differences between healthy volunteers and renal disease patients requires age- and sex-matched controls and a large sample of renal disease patients encompassing the wide variety of renal diseases, as chronic kidney disease is a highly heterogeneous disease group with different underlying pathologies and stages.<sup>21</sup> Native renal T<sub>1</sub> mapping could be of added value to the renal diagnostic arsenal, considering it facilitates direct quantification of renal tissue and enables assessment of regional variances noninvasively. To what extent renal T<sub>1</sub> mapping could truly influence clinical decision-making compared to currently available renal function markers and other new MR techniques such as diffusion-weighted imaging, and blood-oxygen-level-dependent imaging, remains to be investigated, and further histological validation of renal T<sub>1</sub> mapping for tissue characterization is warranted. In the present study we used the same 5(3)3 MOLLI scheme as in cardiac MRI because of practical advantages for clinical implementation; however, other T<sub>1</sub> mapping acquisition protocols might provide more



accurate renal  $T_1$  measurements, since MOLLI measurements are known to be influenced by  $T_2$ -dependence, magnetization transfer effect, and inversion efficiency.<sup>22</sup> Further research is needed to correlate renal native  $T_1$  values with disease severity based on histopathology, and whether renal native  $T_1$  mapping has added value for clinical decision-making. In addition, more studies are needed to assess the reproducibility of renal native  $T_1$  mapping at different imaging centers with various MRI scanner manufacturers, in order to compare current measurements to other centers and to establish normal reference values.

In conclusion, renal native  $T_1$  mapping is a promising technique for renal tissue characterization with good–strong intra- and interexamination reproducibility. Further research is needed to correlate renal native  $T_1$  values with histologic disease severity, and to determine the impact on clinical decision-making.

## References

1. Porrini E, Ruggenti P, Mogensen CE, et al. ERA-EDTA diabetes working group. Non-proteinuric pathways in loss of renal function in patients with type 2 diabetes. *Lancet Diabetes Endocrinol* 2015;3:382–391.
2. O'Neill WC. Structure, not just function. *Kidney Int* 2014;85:503–505.
3. Grenier N, Merville P, Combe C. Radiologic imaging of the renal parenchyma structure and function. *Nat Rev Nephrol* 2016;12:348–359.
4. Taylor AJ, Salerno M, Dharmakumar R, Jerosch-Herold M. T1 mapping: Basic techniques and clinical applications. *JACC Cardiovasc Imaging* 2016;9:67–81.
5. Hueper K, Peperhove M, Rong S, et al. T1-mapping for assessment of ischemia-induced acute kidney injury and prediction of chronic kidney disease in mice. *Eur Radiol* 2014;24:2252–2260.
6. Hueper K, Hensen B, Gutberlet M, et al. Kidney transplantation: Multiparametric functional magnetic resonance imaging for assessment of renal allograft pathophysiology in mice. *Invest Radiol* 2016;51:58–65.
7. Tewes S, Gueler F, Chen R, et al. Functional MRI for characterization of renal perfusion impairment and edema formation due to acute kidney injury in different mouse strains. *PLoS One* 2017;12:e0173248.
8. Friedli I, Crowe LA, Berchtold L, et al. New magnetic resonance imaging index for renal fibrosis assessment: A comparison between diffusion-weighted imaging and T1 mapping with histological validation. *Sci Rep* 2016;6:30088.
9. Peperhove M, Vo Chieu VD, Jang MS, et al. Assessment of acute kidney injury with T1 mapping MRI following solid organ transplantation. *Eur Radiol* 2018;28:44–50.
10. Kellman P, Hansen MS. T1-mapping in the heart: accuracy and precision. *J Cardiovasc Magn Reson* 2014;16:2.
11. Messroghli DR, Radjenovic A, Kozerke S, Higgins DM, Sivanathan MU, Ridgway JP. Modified Look-Locker inversion recovery (MOLLI) for high-resolution T1 mapping of the heart. *Magn Reson Med* 2004;52:141–146.
12. Kellman P, Herzka DA, Arai AE, Hansen MS. Influence of Off-resonance in myocardial T1-mapping using SSFP based MOLLI method. *J Cardiovasc Magn Reson* 2013;15:63.
13. McGraw KO, Wong SP. Forming inferences about some intraclass correlation coefficients. *Psychol Methods* 1996;1:30.
14. Bland JM, Altman DG. Statistical methods for assessing agreement between two methods of clinical measurement. *Lancet* 1986;1:307–310.
15. Lee VS, Kaur M, Bokacheva L, et al. What causes diminished corticomedullary differentiation in renal insufficiency? *J Magn Reson Imaging* 2007;25:790–795.
16. Lemley KV, KRLz W. Anatomy of the renal interstitium. *Kidney Int* 1991;39:370–381.
17. Bohle A, Grund KE, Mackensen S, Tolon M. Correlations between renal interstitium and level of serum creatinine. Morphometric investigations of biopsies in perimembranous glomerulonephritis. *Virch Arch A Pathol Anat Histol* 1977;373:15–22.
18. Bohle A, von Gise H, Mackensen-Haen S, Stark-Jakob B. The obliteration of the postglomerular capillaries and its influence upon the function of both glomeruli and tubuli. Functional interpretation of morphologic findings. *Klin Wochenschr* 1981;59:1043–1051.
19. Zeisberg M, Kalluri R. Physiology of the renal interstitium. *Clin J Am Soc Nephrol* 2015;10:1831–1840.
20. Nath KA. Tubulointerstitial changes as a major determinant in the progression of renal damage. *Am J Kidney Dis* 1992;20:1–17.
21. Levey AS, Coresh J. Chronic kidney disease. *Lancet* 2012;379:165–180.
22. Roujol S, Weingärtner S, Foppa M, et al. Accuracy, precision, and reproducibility of four T1 mapping sequences: A head-to-head comparison of MOLLI, ShMOLLI, SASHA, and SAPHIRE. *Radiology* 2014;272:683–689.